10. G. Reuter *et al.*, *J. Biol. Chem.* **278**, 35193 (2003).
11. H. W. van Veen, C. F. Higgins, W. N. Konings, *Res. Microbiol.* **152**, 365 (2001).
12. G. Chang, C. B. Roth, *Science* **293**, 1793 (2001).
13. G. Chang, *J. Mol. Biol.* **330**, 419 (2003).
14. C. F. Higgins, K. J. Linton, *Science* **293**, 1782 (2001).
15. T. W. Loo, D. M. Clarke, *J. Biol. Chem.* **271**, 27482 (1996).
16. T. W. Loo, D. M. Clarke, *J. Biol. Chem.* **276**, 31800 (2001).
17. M. Seigneuret, A. Garnier-Suillerot, *J. Biol. Chem.* **278**, 30115 (2003).
18. D. R. Stenham *et al.*, *FASEB J.* **17**, 2287 (2003).
19. Starting with a cysteine-less MsbA background where the two native cysteines were replaced with alanines, we constructed 116 single-cysteine mutants. Only four mutations resulted in either weak or no expression (51, 53, 282) or slow aggregation after reaction with the spin label (78). MsbA mutants were spin labeled after Ni affinity chromatography, purified by size-exclusion chromatography (SEC) and then reconstituted in unilamellar vesicles. Details of the structural and functional analysis of the mutants are in the supporting material available on *Science* Online.
20. W. L. Hubbell, H. S. Mchaourab, C. Altenbach, M. A. Lietzow, *Structure* **4**, 779 (1996).
21. The collision frequency with paramagnetic reagents was deduced from the analysis of the saturation behavior of the spin label at each site. Power saturation curves were obtained under nitrogen gas, in the presence of 20% oxygen, or under nitrogen and in the presence of 50 mM NiEDDA. Distinct patterns of oxygen accessibility are expected for transmembrane segments, whereas exposure to the aqueous environments results in high NiEDDA accessibility. Spin-label mobility was estimated from the inverse of the central line width.
22. J. Dong, H. S. Mchaourab, unpublished observations.
23. G. J. Poelarends, W. N. Konings, *J. Biol. Chem.* **277**, 42891 (2002).
24. T. W. Loo, M. C. Bartlett, D. M. Clarke, *Biochemistry* **43**, 12081 (2004).
25. A. H. Buchaklian, A. L. Funk, C. S. Klug, *Biochemistry* **43**, 8600 (2004).
26. C. L. Reyes, G. Chang, *Science* **308**, 1028 (2005).
27. W. T. Doerrler, H. S. Gibbons, C. R. Raetz, *J. Biol. Chem.* **279**, 45102 (2004).
28. A. L. Davidson, *J. Bacteriol.* **184**, 1225 (2002).
29. I. L. Urbatsch, G. A. Tyndall, G. Tombline, A. E. Senior, *J. Biol. Chem.* **278**, 23171 (2003).
30. P. Mitchell, *Nature* **180**, 134 (1957).
31. P. Mitchell, *Res. Microbiol.* **141**, 286 (1990).
32. M. F. Rosenberg *et al.*, *EMBO J.* **20**, 5615 (2001).
33. P. C. Smith *et al.*, *Mol. Cell* **10**, 139 (2002).
34. E. F. Pettersen *et al.*, *J. Comput. Chem.* **25**, 1605 (2004).
35. We thank D. Piston, A. Beth, C. Cobb, H. Koteiche, and R. Nakamoto for critically reading the manuscript. This work was supported by a discovery grant from Vanderbilt University.

Supporting Online Material
www.sciencemag.org/cgi/content/full/308/5724/1023/DC1
Materials and Methods
Figs. S1 and S2
Table S1
References and Notes

21 October 2004; accepted 22 February 2005
10.1126/science.1106592

Structure of the ABC Transporter MsbA in Complex with ADP·Vanadate and Lipopolysaccharide

Christopher L. Reyes and Geoffrey Chang*

Select members of the adenosine triphosphate (ATP)–binding cassette (ABC) transporter family couple ATP binding and hydrolysis to substrate efflux and confer multidrug resistance. We have determined the x-ray structure of MsbA in complex with magnesium, adenosine diphosphate, and inorganic vanadate ($Mg{\cdot}ADP{\cdot}V_i$) and the rough-chemotype lipopolysaccharide, Ra LPS. The structure supports a model involving a rigid-body torque of the two transmembrane domains during ATP hydrolysis and suggests a mechanism by which the nucleotide-binding domain communicates with the transmembrane domain. We propose a lipid "flip-flop" mechanism in which the sugar groups are sequestered in the chamber while the hydrophobic tails are dragged through the lipid bilayer.

Multidrug resistance is an alarming and rapidly growing obstacle in the treatment of infectious diseases, human immunodeficiency virus (HIV), malaria, and cancer (*1*). Drug-resistant bacterial strains that cause gonorrhea, pneumonia, cholera, and tuberculosis are widespread and difficult to treat (*2*). In humans, a similar drug efflux mechanism is a major reason for the failure of several chemotherapeutics in the treatment of cancers. Found ubiquitously in both bacteria and humans, ABC transporters have been implicated in both antibiotic and cancer drug resistance and represent key targets for the development of agents to reverse multidrug resistance (*3*, *4*). Several MDR ABC efflux pumps have been shown to extrude both lipids and drug molecules, which suggests a common transport mechanism for amphipathic compounds across the cell membrane (*5*, *6*).

Department of Molecular Biology, The Scripps Research Institute, 10550 North Torrey Pines Road CB105, La Jolla, CA 92137, USA.

*To whom correspondence should be addressed. E-mail: gchang@scripps.edu

MsbA is an essential bacterial ABC transporter that transports lipid A and lipopolysaccharide (LPS) to the outer membrane (*7–10*) and that has been shown to have overlapping substrate specificity with the multidrug-resistant ABC (MDR ABC) transporter LmrA and with human P-glycoprotein (P-gp) (*11*). MsbA adenosine triphosphatase (ATPase) hydrolysis is stimulated by LPS and lipid A and also shows vanadate-inhibited activity (*12*). LPS makes up the outer leaflet of the outer membrane in Gram-negative bacteria and potently activates the mammalian innate immune system in response to bacterial infections; it can cause septic shock (*13–15*). ABC transporters are minimally composed of two transmembrane domains (TMDs) that encode substrate specificity and a pair of nucleotide-binding domains (NBDs) with conserved structural features. Comparison of the x-ray structures of MsbA and the vitamin B_{12} ABC importer, BtuCD, suggests that differences in substrate specificities are a consequence of structurally divergent TMDs (*16–18*). These structures, along with those derived from electron microscopy (EM) of other MDR ABC transporters, reveal that large conformational changes are possible in both the TMDs and NBDs (*19–23*).

Despite attempts to model the structural changes of MsbA and other MDR ABC transporters, a detailed view of conformational rearrangements during ATP hydrolysis and substrate translocation has remained elusive (*24*). What are the conformational changes of the TMDs during the catalytic cycle? What residues are involved in substrate binding and release? And what specific role does nucleotide binding and hydrolysis play during the catalytic cycle? To address these questions, we describe the structure of MsbA from *Salmonella typhimurium* in complex with adenosine 5′-diphosphate and inorganic vanadate ($ADP{\cdot}V_i$), Mg^{2+}, and rough-chemotype (Ra) lipopolysaccharide (Ra LPS). The structure provides evidence for an intermediate after ATP hydrolysis and a molecular basis for coupling ATP hydrolysis with amphipathic substrate transport.

Crystals of MsbA in complex with $Mg{\cdot}ADP{\cdot}V_i$ and Ra LPS were grown using detergent-solubilized protein incubated with Ra LPS purified from *S. typhimurium*. ATP, Mg^{2+}, and boiled sodium orthovanadate were added to favor the transition state conformation before crystallization (*25*). Mass spectrometry on washed crystals indicated the presence of Ra LPS, nucleotide, and vanadate. The structure was determined by single-wavelength anomalous dispersion (SAD), and the electron density maps were improved by using noncrystallographic symmetry averaging to a resolution of 4.2 Å (see table S1) (*26*). The asymmetric unit revealed two dimers of MsbA with clear electron density corresponding to a nucleotide and Ra LPS. The TMDs in each dimer exhibit a 30° torque relative to the molecular two-fold axis and an extensive interdigitation of the helices (Fig. 1, A and B). A chemical model with good geometry was built with R_{cryst} of 28% and R_{free} of 33%.

In this structure, each dimer contains two bound LPS molecules located at the protein-

membrane interface on the outer membrane leaflet side with the sugar head groups roughly parallel to the axis of the elbow helix (residues 10 to 24) (Fig. 1C). Electron density was observed for only one nucleotide per dimer in the active site position (Fig. 1D). To confirm the positioning of the ADP at this resolution, we replaced ATP with a 2′-brominated ATP analog (*27*) and collected anomalous diffraction data at the bromine edge (λ = 0.9198 Å). Anomalous difference Fourier synthesis using experimental protein phases yielded only one bromine peak (~5 σ) per NDB dimer corresponding to the observed electron density for the nucleotide at the 2′ position (Fig. 1D). The position of the vanadium was confirmed by anomalous Fourier synthesis from diffraction data collected at the vanadium edge (λ = 2.2608 Å). The vanadium peak (~4 σ) corresponds to the position predicted on the basis of the Mg·ADP·V_i structure of myosin (*28*). At this resolution, we have not included either the coordinated oxygen atoms of the vanadate ion or Mg^{2+} in the model described here.

Previous structures have shown MsbA in open and closed conformations in the absence of nucleotide. In the open conformation, the two TMDs interact at the extracellular ends of the membrane-spanning helices to form an inverted V-shaped molecule with NBDs distant from each other. In the closed apo conformation, both the TMDs and the NBDs are closely packed. In addition, a large internal chamber accessible from the cytoplasm is formed between the interacting TMDs (Fig. 2A). The two structures suggest a highly dynamic sampling of conformational space by the protein in the absence of nucleotide with respect to the TMD interactions, lipid bilayer arrangements, and the folding of the NBDs. Electron paramagnetic resonance (EPR) studies also indicate that movements in the TMD are dramatic (*29*, *30*).

Changes in the TMD interactions provide insight into the pathway of substrate efflux. In comparison with the apo closed conformation of MsbA, this structure exhibits a large rigid-body rotation and translation that result in a ~15 Å opening toward the periplasmic ends and a ~15 Å closing of the NBD-associated intracellular domain helices (ICD1; residues 111 to 121), which allow accessibility to an internal chamber from the periplasm but not from the cytoplasm (Fig. 2B). The third extracellular loops (EC3) mediate the internal contact between the two monomers while placing the periplasmic ends of the TM5 helices close together. This causes the periplasmic opening of the internal chamber to be pinched and divides the opening of the cavity into two lobes adjacent to TM6, which corresponds to drug-binding sites observed for LmrA (*31*) and human P-gp (*32*). In this structure, TM5 forms extensive intermolecular interactions with TM2 and TM3. Because the ICD1 is formed between TM2 and TM3, this interaction suggests a probable pathway for transmitting conformational changes caused by ATP hydrolysis to the substrate-binding sites.

Besides affecting the interactions between TMDs, substrate binding and ATP hydrolysis also drive changes in the intermolecular helical packing of the TMDs. Although the TM1 to TM4 helices are arranged in an overall architecture similar to both the open and closed apo conformations, TM5 and TM6 reveal significant rearrangements [root mean square deviation (RMSD) on Cα of 2.1 Å (open) and 1.9 Å (closed)] (Fig. 2C). In both apo structures, a conserved residue (Ile^{257} of *S. typhimurium* MsbA) is located near a helical bulge that characterizes TM5. In this structure, this region has moved toward the interior of the TMD, which facilitates intermolecular contacts within the dimer. Similarly, the periplasmic end of TM6 has moved out of the interior, contributing to a >7 Å shift in EC3 between the apo and post hydrolysis intermediate conformation. The consequence of these intermolecular movements is a concerted movement of TM1, TM6, and the elbow helix toward the cell membrane.

A critical question is how substrate specificity is shared within the subfamily of MDR ABC flippases. In this structure, we observe bound LPS on the outer membrane leaflet side of MsbA forming extensive contacts with TM1 and TM6 from one monomer and with TM2 from the other monomer (Fig. 2D). The hy-

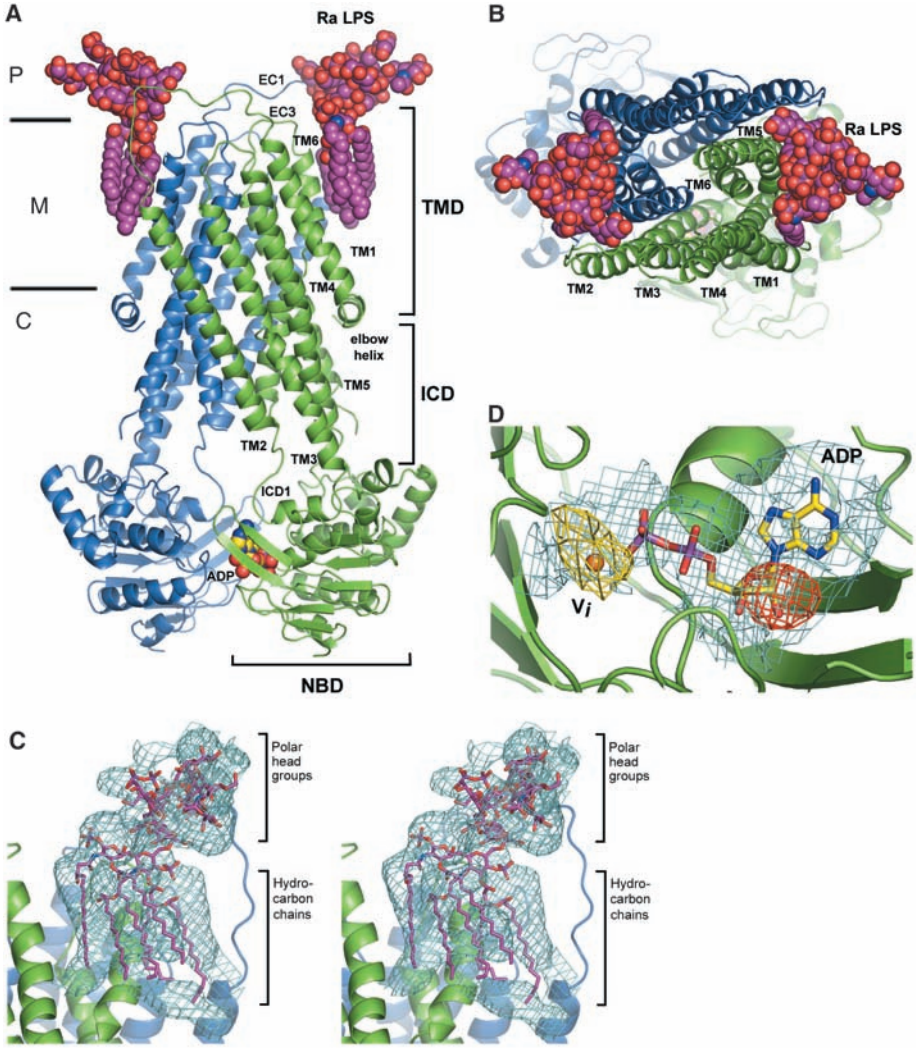

Fig. 1. Structure of MsbA with Mg·ADP·Vi and LPS. (**A** and **B**) The MsbA homodimer is shown in two orthogonal orientations, within the plane of the bilayer and down the two fold, respectively. Green and blue indicate the two monomers. The TMDs span the lipid bilayer matrix (M), and the NBD forms an extensive homodimeric interface within the cytoplasm (C). Two Ra lipopolysaccharide (LPS) molecules (carbon shown in magenta, oxygen in red, nitrogen in blue) are bound on the periplasmic side (P) of the TMDs. A single ADP molecule (carbon shown in yellow, oxygen in red, nitrogen in blue, phosphate in purple) is sequestered within the NBD composite active site. (**C**) Experimental electron density map (1.0 σ) corresponding to bound LPS. (**D**) Experimental electron density map in blue (1.0 σ) surrounding ADP with anomalous difference maps shown in red (4.0 σ) corresponding to the 2′-ADP position for Br and in orange corresponding to the vanadate position (4.0 σ). The images were created with PyMol (*37*).

drocarbon chains of the LPS interact with apolar residues on this interface, and the head groups interact with polar residues near the periplasmic side of the TMD, which includes the first extracellular loop, EC1 (residues 54 to 68). Interestingly, several conserved residues between MsbA and P-gp map to the binding interface of the LPS, which suggests that this region could be a general binding site for other amphipathic compounds. These residues are localized on the elbow helix, TM1, and TM6. Conserved residues specific to the MsbA subfamily also map to the EC1 loop, which interacts with the LPS sugar head groups from opposing monomers, and to the elbow helix (Fig. 2D).

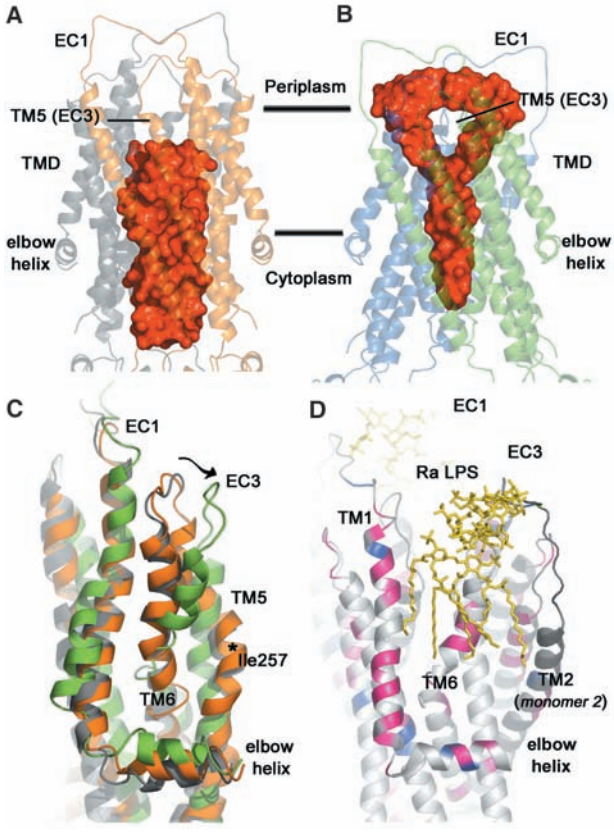

Fig. 2. Transmembrane domain rearrangements and specificity. (**A**) Solvent-filled internal chamber (red) for the closed apo structure of MsbA (monomers in orange and gray). (**B**) Solvent-filled internal chamber for MsbA complexed with LPS and ADP·V_i (monomers in green and blue). (**C**) Superimposed TMDs from open apo (gray), closed apo (orange), and post hydrolysis conformation of MsbA (green) show the movement of TM5, TM6, and EC3 (as indicated by arrow). The helical bulge near residue Ile^{257} is indicated by an asterisk. (**D**) Position of conserved residues shared by MsbA and P-gp (pink) and conserved residues specific to the MsbA subfamily (blue) mapped onto the structure of MsbA (white). The LPS is shown in yellow.

The architecture of the NBDs observed in this model is reminiscent of the dimer sandwich structures of the ABC transporters BtuCD and MJ0796 (*33*) with the P loop and the "LSGGQ" signature motif anchoring two subdomains of the NBD (Fig. 3, A and B). In the ATP-bound form of the MJ0796 NBD dimer, the two motifs from opposing NBDs align to orient the bound ATP molecules and to form a composite active site. In this structure, a nucleotide is observed in only one of the active sites. In addition, the signature motif from opposing NBDs disengages from the P loop and bound nucleotide. We interpret this to imply a post hydrolysis conformation, and it is likely that the nucleotide from the empty binding site has already dissociated.

Interaction between the NBDs and the TMDs involves two conserved motifs. The Q loop contains a conserved glutamine that coordinates Mg^{2+} and the proposed nucleophilic water (*34*), and the short conserved ICD1 helix mediates the contacts with the proximal NBD and the TMD. In the apo structure of BtuCD, the ICD1-equivalent helix (termed the L loop) does not contact the conserved glutamine (Gln^{80}) in the Q loop (Fig. 3C). However, in the structure described here, the amino end of the ICD1 (residues 111 to 121) is in position to interact with the glutamine from the Q loop and fits

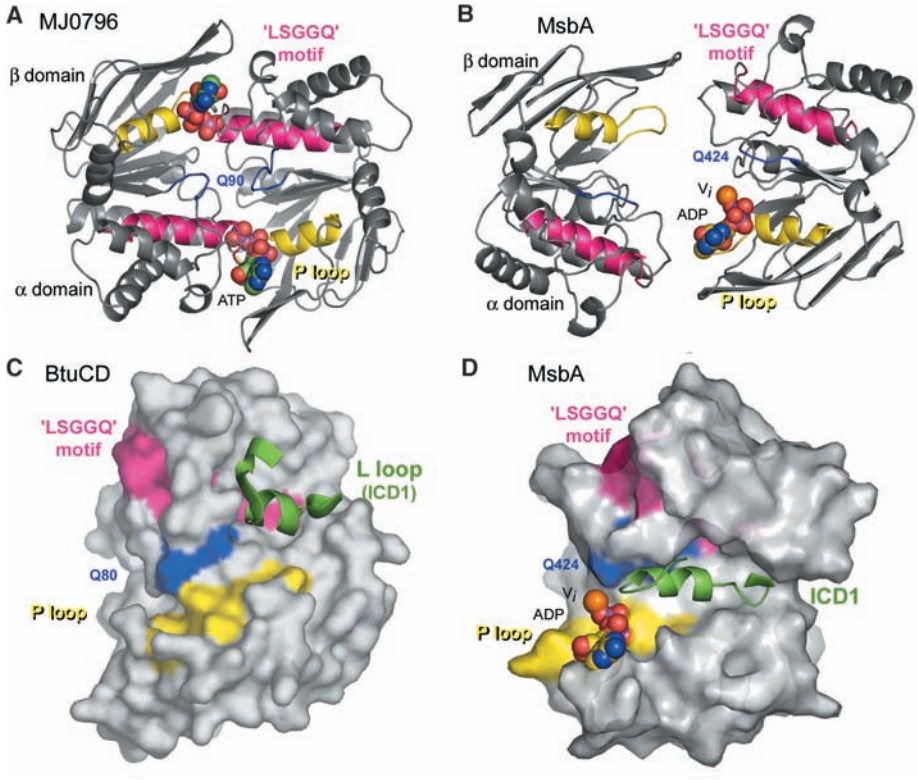

Fig. 3. The composite catalytic site of the NBDs with substrate and conserved sequence motifs. (**A**) Two bound ATP molecules (carbon shown in green, oxygen in red, nitrogen in blue, phosphate in purple) are sandwiched between the P loop (yellow) and LSGGQ (pink) moieties in the composite active site from MJ0796. The Q loop is shown in blue. (**B**) Architecture of interacting NBDs from MsbA post hydrolysis intermediate showing one bound ADP (carbon shown in yellow, oxygen in red, nitrogen in blue, phosphate in purple) molecule and one vanadate (orange) per dimer. The nucleotide is bound to the P loop (yellow) and disengaged from the conserved LSGGQ signature motif from the opposing monomer (pink). The Q loop is shown in blue. (**C**) Surface view of a single NBD from the apo structure of BtuCD shows no interaction between the L loop and the conserved glutamine (Gln^{80}) (blue) that is proposed to coordinate the nucleophilic attacking water (L loop is the ICD1 equivalent, shown in green). (**D**) Post hydrolysis intermediate MsbA shows the ICD1 helix (green) from the TMD positioned to interact with conserved glutamine (Gln^{424}) (blue).

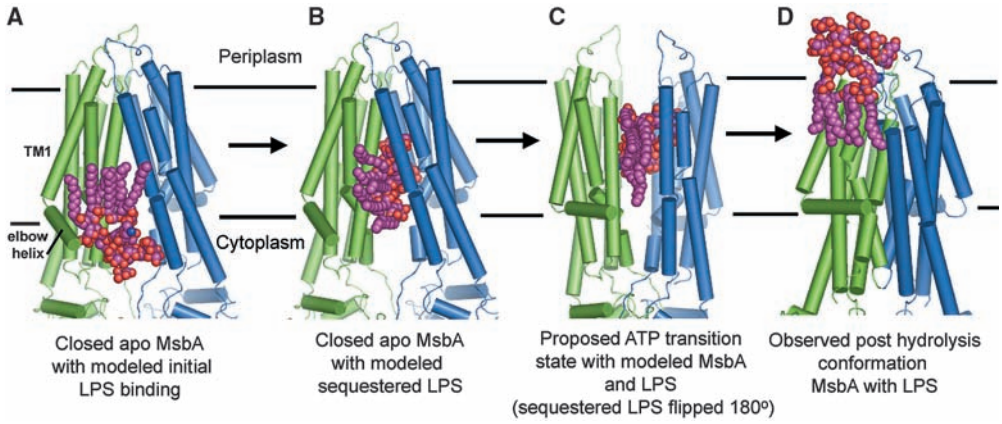

Fig. 4. Proposed model for sequestering polar sugar head group of the LPS in internal chamber of MsbA (only one LPS shown for clarity). (**A**) LPS initially binds to the elbow helix as modeled onto the closed apo structure. (**B**) Lipid head groups are modeled to insert into the chamber of the apo closed structure. (**C**) As the transporter undergoes conformational changes related to binding and hydrolysis of ATP, the head group is flipped within the polar chamber while the LPS hydrocarbon chains are freely exposed and dragged through the lipid bilayer. Both LPS and MsbA conformations are modeled. (**D**) LPS is presented to the outer leaflet of the membrane as observed in this structure.

within an elongated groove on the TMD-exposed NBD surface (Fig. 3D). As ICD1 is the only structural motif from the TMD to interact with the active site of the NBD, it seems likely that a reorientation of the ICD1 helix to contact with the Q loop could depend on the catalytic status of the γ-phosphate.

Together with previously described MsbA structures, the model described here provides a framework for interpreting functional data concerning MDR ABC transporters. Substrate recognition by the TMD and nucleotide binding by the NBD change the conformation of the molecule and thus promote the formation of the NBD dimer in an arrangement competent to hydrolyze ATP. This dimerization of the NBDs and hydrolysis of ATP together are the "power stroke" of the transport cycle and drive the transport of the lipid substrate from the inner to the outer membrane leaflet through conformational changes in the TMDs. In the post hydrolysis conformation structure described here, only one ADP is trapped per dimer, which suggests that the two NBDs act to hydrolyze ATP alternately. This would support the model of alternating catalytic sites proposed for P-gp (*35*) and LmrA (*36*). However, the presence of two LPS molecules on the outer leaflet side of the membrane suggests two substrate molecules may be transported per power stroke.

We propose a structurally based mechanism of LPS flipping whereby the sugar head groups are sequestered and "flipped" in the internal chamber while the hydrophobic tail of the lipid is dragged through the bilayer. We have observed a titratable high-affinity binding site for several cationic heavy metals such as 2-chloromercuri-4-nitrophenol and ethyl mercury chloride located at the interface of the elbow helix and TM1 (*25*). We propose that this region, which contains a locus of conserved residues across this subfamily of MDR ABC transporters, may point to an initial high-affinity surface binding site for LPS and other cationic hydrophobic compounds similar in chemical structure to most anticancer chemotherapeutics. In our proposal, LPS initially binds near the elbow helix (Fig. 4A). During the power-stroke step, the sugar head groups are sequestered within the chamber and flipped to the outer membrane leaflet by the rigid-body shearing of the TMDs while the hydrophobic tails of the LPS are dragged through the lipid bilayer (Fig. 4, B and C). The result is an energetically favorable "flip-flop" in the orientation of the lipid in the bilayer and the presentation of LPS sugar head groups on the periplasmic side of the membrane (Fig. 4D), as observed in this structure.

The size of the chamber is large enough to accommodate the sugar groups from two Ra LPS molecules. The head group size of various LPS and related molecules affects the stimulation of MsbA ATPase activity. A larger stimulatory effect on ATP activity is observed for Re LPS, which has a shorter head group than that for Ra LPS. This might be an effect of steric hindrance inside the cavity to accommodate the sugar head groups. Our model could also extend to other molecules with cationic/hydrophobic properties, such as most chemotherapeutic drugs associated with multidrug resistance. A mechanism where export could occur more exclusively through the chamber for less hydrophobic molecules is certainly possible. The model described constitutes a general molecular basis for export by MDR ABC flippases and the structural characterization of a Mg·ADP·V_i post hydrolysis conformation of MsbA, which provides an excellent springboard for further studies.

References and Notes

1. R. C. Moellering Jr., *Clin. Infect. Dis.* **27** (suppl. 1), S135 (1998).
2. M. Ouellette, D. Legare, B. Papadopoulou, *J. Mol. Microbiol. Biotechnol.* **3**, 201 (2001).
3. M. Dean, R. Allikmets, *J. Bioenerg. Biomembr.* **33**, 475 (2001).
4. H. W. van Veen, C. F. Higgins, W. N. Konings, *Res. Microbiol.* **152**, 365 (2001).
5. V. Ling, *Cancer* **69**, 2603 (1992).
6. Y. Raviv, H. Pollard, E. P. Bruggermann, I. Pastan, M. M. Gottesman, *J. Biol. Chem.* **265**, 3975 (1990).
7. M. Karow, C. Georgopoulos, *Mol. Microbiol.* **7**, 69 (1993).
8. A. Polissi, C. Georgopoulos, *Mol. Microbiol.* **20**, 1221 (1996).
9. Z. Zhou, K. A. White, A. Polissi, C. Georgopoulos, C. R. Raetz, *J. Biol. Chem.* **273**, 12466 (1998).
10. G. Reuter *et al.*, *J. Biol. Chem.* **278**, 35193 (2003).
11. W. T. Doerrler, H. S. Gibbons, C. R. Raetz, *J. Biol. Chem.* **279**, 45102 (2004).
12. W. T. Doerrler, C. R. Raetz, *J. Biol. Chem.* **277**, 36697 (2002).
13. R. Medzhitov, C. A. Janeway, *Cell* **91**, 295 (1997).
14. J. A. Hoffmann, F. C. Kafatos, C. A. Janeway, R. A. Ezekowitz, *Science* **284**, 1313 (1999).
15. C. R. Raetz, C. Whitfield, *Annu. Rev. Biochem.* **71**, 635 (2002).
16. G. Chang, C. B. Roth, *Science* **293**, 1793 (2001).
17. K. P. Locher, A. T. Lee, D. C. Rees, *Science* **296**, 1091 (2002).
18. G. Chang, *J. Mol. Biol.* **330**, 419 (2003).
19. M. F. Rosenberg, R. Callaghan, S. Modok, C. F. Higgins, R. C. Ford, *J. Biol. Chem.* **280**, 2857 (2005).
20. A. Ferreira-Pereira *et al.*, *J. Biol. Chem.* **278**, 11995 (2003).
21. J. Y. Lee, I. L. Urbatsch, A. E. Senior, S. Wilkens, *J. Biol. Chem.* **277**, 40125 (2002).
22. M. Chami *et al.*, *J. Mol. Biol.* **315**, 1075 (2002).
23. M. F. Rosenberg *et al.*, *EMBO J.* **20**, 5615 (2001).
24. C. F. Higgins, K. J. Linton, *Nat. Struct. Mol. Biol.* **11**, 918 (2004).
25. Materials and methods are available as supporting material on *Science* Online.
26. C. R. Reyes, G. Chang, unpublished observations.
27. M. Gruen *et al.*, *Protein Sci.* **8**, 2524 (1999).
28. C. A. Smith, I. Rayment, *Biochemistry* **35**, 5404 (1996).
29. J. Dong, G. Yang, H. S. Mchaourab, *Science* **308**, 1023 (2005).
30. A. H. Buchaklian, A. L. Funk, C. S. Klug, *Biochemistry* **43**, 8600 (2004).
31. G. F. Ecker *et al.*, *Mol. Pharmacol.* **66**, 1169 (2004).
32. T. W. Loo, D. M. Clarke, *J. Biol. Chem.* **276**, 14972 (2001).
33. P. C. Smith *et al.*, *Mol. Cell* **10**, 139 (2002).
34. K. P. Hopfner *et al.*, *Cell* **101**, 789 (2000).
35. A. E. Senior, D. C. Gadsby, *Semin. Cancer Biol.* **8**, 143 (1997).
36. H. W. van Veen, A. Margolles, M. Muller, C. F. Higgins, W. N. Konings, *EMBO J.* **19**, 2503 (2000).
37. W. L. Delano, www.pymol.org (2002).

38. We thank P. Wright, D. C. Rees, R. Stroud, I. Urbatsch, W. Balch, R. Milligan, and R. H. Spencer for discussion and comments on the manuscript, as well as O. Pornillos, Y. Yin, and A. Ward. We also thank the Stanford Synchrotron Radiation Laboratory, Advanced Light Source, and Advanced Photon Source for the tremendous support and access. C.L.R. was supported by a NSF Minority Postdoctoral Fellowship. This work was supported by NIH grant GM61905, Beckman Young Investigators Grant, Fannie E. Rippel Foundation, Baxter Foundation, and The Skaggs Institute for Chemical Biology. Coordinates have been deposited in the Protein Data Bank (accession code 1Z2R).

Supporting Online Material

www.sciencemag.org/cgi/content/full/308/5724/1028/DC1
Materials and Methods
Table S1
References and Notes

19 November 2004; accepted 11 March 2005
10.1126/science.1107733